Journal of Electric Propulsion

RESEARCH Open Access

Characterization of the ion beam and thrust vector of a 5-kW hall effect thruster using a hemispherical sweep probe apparatus

Chhavi Chhavi[1*] and Mitchell L. R. Walker[1]

*Correspondence:
Chhavi Chhavi
chhavi@gatech.edu
[1]Georgia Institute of Technology, Atlanta, GA 30332, USA

Abstract

Any manufacturing flaw in Hall effect thruster (HET) components may distort plasma characteristics and thruster performance. The High-Power Electric Propulsion Laboratory of the Georgia Institute of Technology developed a hemispherical sweep apparatus to characterize the three-dimensional ion beam current of the plasma plume. The sweep probe apparatus sweeps a Faraday probe in the vertical and horizontal direction at a constant radius of 1 m across the HET plume to measure the three-dimensional ion current density. The sweep probe is utilized to take measurements of the P5 HET operating at 300 V, 7.9 A on krypton propellant under uniform and azimuthally non-uniform magnetic field configurations in vacuum facility with operational pressure of 3.1×10^{-6} Torr-Kr. In the uniform magnetic field configuration, the measurements show that the plume center is 4° below the thruster center, a feature not captured by the horizontal sweep of the Faraday probe. The ion beam current measured from the three-dimensional sweep probe apparatus exhibited a 0.03% decrease compared to the conventional horizontal scan using the Sweep Probe Apparatus, whereas the divergence angle showed a 4% variation. In the non-uniform magnetic field configuration, 0.36 G/° azimuthal gradient in the channel, the measurements identified a 24% decrease in ion beam current and a 5.8° spatial deviation of the thrust vector. The sweep apparatus enables an improvement in the ion beam current measurement through three-dimensional plume mapping, plume non-uniformity detection, and thrust vector characterization.

Keywords Hall effect thruster, Thrust vector, Three-dimensional, Sweep probe apparatus, Diagnostics, Hemispherical, Ion beam current

Introduction

Hall effect thrusters (HETs) are electrostatic devices that accelerate propellant by ionizing the particles and by using an axial electric field [1]. The acceleration of the ionized propellant particles out of the HET channel generates the necessary thrust for orbital maneuvers [2]. An increasing number of satellite operators utilize the HET because of its high specific impulse and high efficiency [3–5]. The rising popularity of HET in the commercial sector contributes to its utilization in propulsion systems for Low Earth

Orbit (LEO), Geosynchronous Earth Orbit (GEO), and interorbital missions [6–9].The thrusters are being mass-produced in response to the rising demand for HETs to provide propulsion for satellite constellations. Although it is relatively easy to produce thrusters in large quantities, it is crucial to conduct acceptance testing to ensure that the HET meets the necessary performance and capability requirements for spaceflight operations prior to integration on the spacecraft. Present-day space missions necessitate propulsion devices with significant power and thrust capabilities. The mass production of HETs increases the likelihood that manufacturing defects will manifest in the HET components, resulting in their inability to pass acceptance tests. The presence of manufacturing defects across various HET components leads to disparities in plasma properties, which subsequently modify the thruster's performance parameters [10]. In addition to altering the plasma parameters and the associated processes, these inconsistencies may cause a variation in the beam centroid and its subsequent deviance from the centerline, leading to an off-axis thrust vector.

Numerous studies have been conducted addressing ion beam current density non-uniformities present in HETs. These non-uniformities arise in HETs due to several manufacturing features, such as non-uniform propellant flow [10], propellant neutral densities [11], anode orifice configurations [12] and electrical shorts. The non-uniformities present in the HETs result in azimuthal variations of plasma properties inside the channel. Extensive experimental study by Hofer [10] using near-field and far field diagnostics demonstrated that ion beam current non- uniformities are strongly couple to propellant flow distribution, neutral dynamics and anode design. In this study, NASA-173 M was operated at conditions 300–1000 V discharge voltage with anode mass flow rate of 2-10 mg/s Xenon. During this wide operational study, the thrust increase from 40mN at low power to 300mN at high power operation with specific impulse of 3500s. Faraday probe utilized to conduct far field plume measurement provided non- axisymmetric ion current density distribution with variations from 10 to 25% along with skewed plume profiles. Corresponding azimuthal variations in plasma potential and electron temperature were also observed using RPA, confirming that the asymmetry is not limited to ion flux alone but is a global plasma effect. Though the asymmetric plume affected the ion beam current density and plume structure, total thrust and efficiency remained insensitive to non- uniformities in propellant flow. However, a detailed three-dimensional profile map of the ion beam current was not obtained to verify the findings. Another experimental study performed by Reid and Gallimore [11] on the neutral flow dynamics established that the azimuthal non -uniformities in neutral density arise naturally from propellant injection geometry and anode design and thus can results in asymmetric electron mobility across the anode. Neutral xenon flow velocities and temperatures measurements obtained using Laser induced fluorescence (LIF) varied from 100 to 200 m/s and 200 to 1600 K respectively across the various axial location. The corresponding ionization mean free path was reported to vary from a few millimeters up to approximately 1 cm, depending on local neutral density and electron temperature. Their work clearly demonstrates that neutral-flow non-uniformity is a dominant experimentally observed driver of azimuthal plasma non-uniformity in operating HETs. Benavides et al. [12] also conducted testing on the NASA H6M-LM to validate the effects of the anode orifice configuration on the ionization uniformity and thruster stability. Through the testing of a high-propellant-throughput design, it was observed that the asymmetric

propellant injection produces variation in the discharge current while redesigned anode flow distributors significantly reduced these asymmetries. The experiments further demonstrated that improved injection symmetry produced measurable increases in discharge stability and beam uniformity, thus demonstrating design dependence of HET performance parameters. While experimental studies were performed on asymmetric propellant, Lazurenko [13] performed a computational study of azimuthal non-uniformities in the magnetic field to evaluate the effect of the azimuthal magnetic field gradient. To address the conditions and consequences of a non-axisymmetric magnetic field in HETs, one of the potential results of asymmetric magnetic fields that was taken into consideration was thrust vectoring. Deviation of thrust vector for SPT-100 by azimuthal magnetic field asymmetry was simulated through the creation of eight additional coils and four additional outer poles at 300 V and 4.5 mg/s of xenon anode flow conditions. Allowing the electron temperature, plasma potential, and neutral number density to be constant and symmetric for inertial wall calculations resulted in a simplified model. The consideration of ion volume recombination was omitted to enhance the model's ease of compilation. Using simulation techniques to analyze the distribution of ion flux density and velocity, visual evidence was obtained supporting the concept of thrust vectoring using asymmetric magnetic field. Though numerous studies have been performed demonstrating the impact of various factors on the plasma plume and thruster performance, high resolution experimental measurement of ion beam to observe the impact of these non-uniformities on thruster vector still remains a challenge.

Several investigations have been carried out to examine and study the thrust vectoring capabilities of the HETs during operation. Various thrust vector measurement systems have been developed utilizing the Faraday probe, double Langmuir, cylinder rods, and retarding potential analyzer (RPA) [14–19]. Thrust vector characterization was conducted by Pollard using four double-wired Langmuir probes aligned in the form of a cross situated 200 cm downstream of the thruster exit plane [18]. A monitoring system utilizing reflective mirrors and charged couple device (CCD) cameras was employed to determine the thruster's centerline. The movement of the ion beam centroid was traced using motorized position monitoring to detect any divergence in the thrust vector. The motorized mechanism was employed to maintain null error signals by equilibrating the current gathered in the two mutually perpendicular axes of the thrust vector measurement device, thereby enabling the tracking of the beam centroid. Nonetheless, the failure to detect the azimuthal ion beam unsymmetric condition and the unexplained systematic mistake leading to an overall thrust loss opened the door for additional research in this area. Polk [19] designed a thrust vector probe comprising 16 vertical and 16 horizontal graphite rods, each with a diameter of 9 mm and a length of 1.2 m. The probe grid was positioned at the far end of the vacuum chamber, enabling uninterrupted beam exposure for long-term testing. A Leica Mancat theodolyte system employed optical technology to precisely measure the alignment between the vector probe and the thruster axis [20]. An exhaustive analysis of the thrust vectoring condition for the Engineering Model Thruster (EMT2), which served as an engineering prototype of the NSTAR thruster, was conducted through 8,000 h of testing. The current obtained by the rods varied during the experiment. Possible causes of the initial thrust vector offsets, such as unsymmetric magnetic fields, have been identified but not thoroughly investigated. Nevertheless, this methodology proved effective in gathering rod current data

that corresponded to ion beam current throughout an extended period of testing using an ion beamlet model [20]. The primary drawback of this design is that measurements are taken at varying radial dimensions due to the planar collecting plane; consequently, to achieve three-dimensional measurements, the probe must be positioned at different radial locations to compile results, which prolongs operational time and leads to inaccuracies. The influence of the high conductive surface area of these rods on floating and plasma potential requires investigation. Reijen [17] created another thrust vectoring device using a retarding potential analyzer (RPA) and energy-selective mass spectroscopy to analyze ion beam current and thrust vectoring. The thrust vector scanner comprised of 37 RPAs mounted in a semicircle configuration on a pole. The boom was designed to provide data 1 m downstream of the thruster exit plane, allowing for far-field plume characteristics. The RPAs enabled the utility of ion selectability at a particular energy level, thereby permitting collections of ions of varying energy levels. Although the use of RPA enabled greater accuracy, it necessitates more prolonged exposure to the plume, leading to the heightened deterioration of RPA grids. The RPA boom construction provided the ability to map the plasma plume fully. Extended exposure of RPA to the plasma plume leads to accelerated deterioration and degradation of the probe, potentially causing measurement inaccuracies and significant testing delays. Additionally, RPA features an electrically intricate architecture, and deploying several such probes can provide complex challenges for three-dimensional measurement. An alternative method, a thrust vectoring device comprising an array of Faraday sensors that maps a portion of the ion beam, was devised by Benavides [14]. The device consists of 23 Faraday probes affixed on a 1-m curved aluminum framework installed on a motorized radial arm. The thrust vectoring device collected data ranging from − 22° to 22°, encompassing approximately 44° of the plasma plume. The thruster vectoring device successfully generated a comprehensive three-dimensional map of the ion beam at various operating conditions for the Advanced Electric Propulsion System (AEPS) HET. The apparatus enabled precise measurements of the beam current and thrust vector while preventing any escalation in the back sputter effect on the thruster. However, to achieve comprehensive three-dimensional measurements, the quantity of probes must significantly exceed 23 Faraday probes. The multi-probe technique requiring more than 23 Faraday sensors becomes a complex system to manage and may provide considerable challenges.

This work presents the design and implementation of a hemispherical sweep apparatus that overcomes the limitations of complex electronic setups with multiple probes and to achieve a broader ion beam coverage. The sweep apparatus, designed to provide the characteristics of a quasi-three-dimensional plasma beam, offers a comprehensive measurement setup for plasma non-uniformities and potential use in studying the thrust vectoring when the thruster is operated in uniform and non-uniform magnetic field configuration. The equipment sweeps a Faraday probe vertically across the HET plume while spanning radially using a radial arm to gather quasi three-dimensional or two-dimensional spherical ion currents of the thruster at different operating conditions at fixed radial distance. The innovative diagnostic apparatus offers a quantitative measurement method for assessing the influence of non-uniformities due to magnetic field and manufacturing errors, on the thrust vector as a function of ion beam current density centroid for HETs. In the current study, the apparatus characterizes the ion beam current of a 5-kW laboratory HET, P5 [21], operating in uniform and non-uniform magnetic

field configuration, having azimuthal magnetic field gradient demonstrating the shift in the precise position of the thruster vector in three-dimensional space due to magnetic field non-uniformities.

Design overview

Design objective

The design objective of the current hemispherical sweep probe apparatus is to provide three-dimensional plume characterization of the HET plasma plume in terms of the ion beam current. The three-dimensional mapping of the ion beam current is provided using the Faraday probe as the primary ion beam current measuring device in the apparatus. For this undertaking, the subsequent objectives and requirements are identified:

1) The diagnostic apparatus enables precise and repeatable characterization to facilitate plume measurement.

The objective establishes the ion flux deviation sensitivity with the need for precise and dependable measurement with less than 2° horizontal and vertical deviations. The methodology used to satisfy the criteria are derived from the guidelines outlined in the recommended practices for precise measurements utilizing the Faraday probe [22]. This criterion restricts measurement uncertainty to less than 2°, enabling the translating mechanism to operate with minimal tremble and optimum position control.

2) Orthogonality must be maintained between the probe collector surface and the ion beam.

The current objective necessitates that the probe collection surface remains orthogonal to the plume to maximize the surface area for ion beam current collection. To facilitate the orthogonality, curved arc with a radial distance of 1 m is to be considered as the circular track path for the probe allowing far field plume measurements. The radial distance is measured from the thruster center to multiple position on the track where the Faraday probe is position to ensure orthogonality is maintained. An error of 5% is allowed as uncertainly associated with measurement and manufacturing of the track. Orthogonality also promotes the reduction of sheath potential effects that occur when ions interact with the collector plate.

3) Capability to provide continuous sweep measurements throughout extended periods of testing.

The objective enables the probe setup to be used for many tests over a long period of time, with the ability to withstand considerable temperature and pressure variations in the vacuum facility environment. Material selection for the apparatus components is done based on their performance in the plasma environment. The requirement necessitates that the probe instrument possesses robustness and longevity to ensure its sustained utilization in the future. The thermal fluctuations should remain below 5° C across the diagnostic throughout the plume measurement allowing for precise characterization of probe position. Thus, allowing for use of anodized aluminum as the key material for the apparatus components allowing for good thermal and electrical isolation.

4) The impact of the probe's presence in the plume on the floating potential of the thruster is negligible.

This objective aims to guide designing the sweep probe apparatus to minimize its impact on the plasma and the thruster operating conditions, ensuring accurate plasma performance characteristics. The size of the components in front of the plasma source is minimized while maintaining structural integrity during the testing operation. The probe shouldn't vary the floating potential of the thruster more than 5% while transversing through the plume. Electrical isolating components along with minimal backscattering material are key properties used to design and select the diagnostic components.

5) Capability to regulate the frequency of measurement or data sweeps of the plume.

The capacity to regulate the frequency of measurements facilitates the acquisition of comprehensive and spatially specific data at the intended locations of interest. To fulfill the requirement, the sweep probe apparatus enables the operator to collect more extensive data sets in concentrated areas, such as the centerline for thrust vectoring or plume endpoints for facility effects. The said operation is achieved using motion controllers and stepper motors. The motion control system should be designed to allow minimum 3 sweeps of probe across the track with less than 2° variation in positioning at any fixed horizontal position.

6) A lightweight, simplistic design featuring minimal back sputtering.

The simplistic, lightweight design of the sweep probe apparatus allows for easy installation and utilization of the setup for various testing conditions and hence is a key requirement. The weight of the diagnostic should be below 150lbs to allow positional accuracy with the motion control system used by radial arm without any deflection. It also increases the data collection capabilities of the testing facility, aiding in the advancement of the understanding of the plasma plume. Usage of simple electromechanical mechanisms for probe propagation allows the objective to be achieved along with the usage of lightweight material such as aluminum.

Design

The design objective provides a detailed requirement needed to be fulfilled by the sweep probe apparatus for successful validation and utilization. These goals are accomplished by the current apparatus consisting of a geared face curved framework/track, a motion-controlled gear, a probe mount, and probe electronics incorporated into the sweep probe apparatus to enable the probe to be swept across the plasma plume. Due to its adaptability and simplicity, the design permits the attachment of diverse probes to acquire plasma properties at distinct locations within the plume. The current design utilizes a Faraday probe to detect the ion beam current across the plume. According to Brown [23] the downstream distances considered for the far field plume measurements should be in the range of 8 to 20 thruster diameter. This allows for minimal systematic error associated with near field geometry along with improved measurement accuracy of ion current density and plume divergence. P5 HET used in the current study has a thruster diameter of 173 mm. The far field plume measurement distance for P5 according to methodology established by Brown [23] approximates to 1 m. To verify whether 1 m works for the current facility and thruster operation, correction factors of distance K_D and angle correction K_A were calculated using the conventional Faraday probe on the radial arm. It was observed that the values of the combined effect (K_D/ K_A) were 1.01 at the centerline

and 1.00 at the end points for radial measurement distance of 1 m. With the correctional being minimal the facility effects are low impact on the measurement thus making the far field measurement more reliable.

Though measurements at varying radial distances were not performed in the current study, previous studies on the P5 hall thruster, as well as the current estimation of the correction factors, indicate the assumption of P5 satisfying the far field at 1 m holds true. In addition, comparison with earlier P5 investigations and measurements is made possible through the measurements performed at 1 m distance [24, 25]. Hence, the apparatus consists of a circular framework with a radius of 1 m, constructed from aluminum 6061, as depicted in Fig. 1. The framework is composed of a geared track on one side and a curved flat surface insulated from the plume using graphite fragments on the other side. A slot is created in the aluminum structure to accommodate motion bearings and preserve the orthogonality of the probe as it moves along the curved trajectory. The bearing linked to the probe mount guarantees that the probe remains in the correct orientation while sweeping through the plume. The geared track framework currently ranges from – 41 to 46 °, providing a measurement span of 87 ° of the plume. The framework can be extended to a 180° span in facilities without spatial restrictions such as floor and the thruster mount. The probe mount is fabricated utilizing a combination of aluminum and graphite components. The aluminum brackets are connected to the motion gear, and the stepper motor is employed for motion control. As depicted in Fig. 1, the Nema 17 motor with a 50:1 ratio planetary gearbox is utilized to translate the probe along a 1-m radius path via a motion gear. The stepper motor enables accurate gear movement along the track due to the precise motion step control and provides positional control over the probe. The stepper motor magnetic field was measured to be less than 0.01 G using a FW Bell Gaussmeter 5080. Therefore, for a 300-eV energy ion, the deflection will be less than 0.2° allowing negligible effect on the ion motion and thus the effect of the motor is neglected in the current study. The graphite component along with insulators of the mount serves the purpose of connecting the Faraday probe to the mount while guaranteeing electrical isolation to other components and reduced interference due to sputtering during measurements, as seen in Fig. 2. The complete sweep probe apparatus assembly weighed around 100lbs satisfying the design requirements. The construction

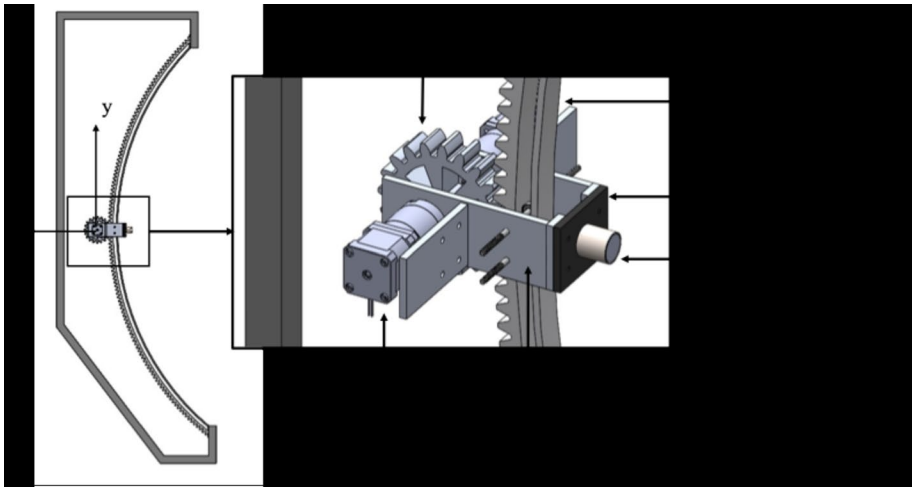

Fig. 1 Detailed rendering of the 1-m curved sweep probe apparatus with its components: Stepper motor, Motion control gear, Gear framework, Faraday probe and Aluminum and graphite mount components

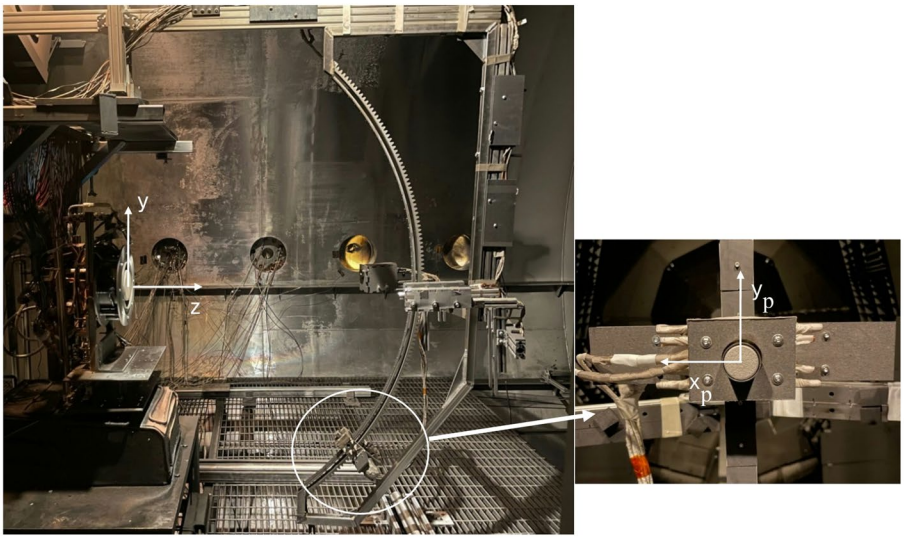

Fig. 2 Picture of the 1-m Curved Sweep Probe Apparatus installed in VTF-2 with coordinate y axis representing direction of gravity. Probe cartesian coordinate system denoted by x_p and $y_p$as shown in the detailed view

of the Faraday probe adheres to the recommended principles, utilizing a stainless-steel casing that is 1 inch in length and a collector coated with tungsten. Faraday probes are flat electrodes specifically designed to measure ion beam current [22]. The probe consists of a 0.62 cm thick cylindrical collector with a diameter of 2.31 cm. The cylindrical guard ring/ casing possesses an outer diameter of 2.54 cm and a wall thickness of 0.074 cm. The collector electrode is negatively biased about the local plasma potential, resulting in the collection of only ions. The plasma potential was specifically determined from distinct Langmuir probe observations in the near-plume area. The Faraday probe bias was established at roughly – 30 V in relation to the local plasma potential, aligning with values documented in the literature for Hall thruster plume investigations. The intended plasma potential was determined by employing a Langmuir probe and a retarding potential analyzer (RPA) to assess the local plasma potential V_p in the plume, at the identical area where the Faraday probe will be positioned (e.g., 1 m downstream). In conventional testing, the Faraday probe crosses the HET plume at a set radial distance, resulting in a spatially specified ion current density distribution function. With the additional degrees of motion, the current apparatus provides a complete three-dimensional mapping of the ion current density distribution using the Faraday probe.

Experiment procedure

Vacuum facility

All investigations are conducted in Vacuum Test Facility 2 (VTF-2) in the High-Power Electric Propulsion Laboratory of the Georgia Institute of Technology. VTF-2 consists of a 9.2 m long stainless-steel chamber with a diameter of 4.9 m [26]. High vacuum is attained using ten liquid nitrogen-cooled CVI TM1200i cryopumps linked to two Stirling Cryogenics SPC-4 compressors. The pressure is measured using one Agilent Bayard-Alpert (BA) 571 hot-filament ion gauges on the chamber flange and two MKS Granville Phillips 370 Stabil-ion gauges located 0.3 m downstream of the thruster exit plane and 0.6 m from the thruster centerline. The Agilent XGS-600 Gauge Controller is utilized to regulate the outer ion gauge, and the Granville Phillips 370 Controller is used to measure

the ion gauges inside the chamber to deliver precise pressure measurements. During testing, the ion gauge inside the chamber recorded nominal operating pressures of 5.9×10^{-6} Torr-N_2 and, 1.1×10^{-5} Torr-N_2, respectively. The ion gauge on the chamber wall recorded nominal operating pressures of 3.6×10^{-6} Torr-N_2. The operational and base pressures were measured and then averaged using the two gauges present inside vacuum chamber due to higher accuracy of measurements near thruster. Subsequently, the operational pressure is adjusted for krypton using a correction method.

$$Poperational - corrected = 1/corr(Poperational - measured - Pbase) + Pbase, \quad (1)$$

with *corr* being equal to 1.96 for krypton [27]. Resulting in the base and operational pressure in the facility is 2.6×10^{-9} Torr-N_2 and 3.1×10^{-6} Torr-Kr.

5-kW hall thruster

The experiment presented in this study is conducted using the P5, a 5-kW laboratory HET P5 built through a collaboration between the Air Force Research Laboratory (AFRL) and the University of Michigan. The P5 HET is used for the experiment due to its comparable performance capabilities to commercial HETs [21]. P5 features a stainless-steel anode with 36 slot holes, a ceramic discharge channel, an inner magnetic core, and eight outer magnetic cores that generate the magnetic field necessary for the functioning of the HET. The thruster comprises a boron nitride and silicon dioxide BN-SiO_2, M26 grade ceramic channel with an outside diameter of 173 mm and channel width of 25 mm [28, 29]. The magnetic circuit architecture of eight outer cores form the outer coil circuit and one inner coil. An EPL-500 hollow cathode is positioned such that the cathode orifice at a distance of 2.2 cm downstream of the P5 exit plane and 7 cm above the centerline at a -35° vertical angular position. The thruster is operated at a discharge voltage of 300 V, an anode flow rate of 5.61 mg/s, and a cathode flow rate of 0.44 mg/s of krypton. Krypton was chosen as the propellant for these investigations to account for facility constraints and diagnostic benefits. Krypton offers more beam divergence and less neutral background density than xenon, enhancing the signal-to-noise ratio for probe measurements and facilitating crisper plume mapping. Its reduced cost and enhanced availability render it particularly suitable for extensive laboratory-scale testing under various situations. Xenon is the standard propellant for Hall thrusters because of its superior ionization efficiency; however krypton provides further insights into performance and plume dynamics with a lighter propellant. All recorded current densities were normalized to compensate for krypton's lower ionization efficiency compared to xenon.

To evaluate the effect of non-uniformities in the magnetic field on ion beam current and thrust vector, the outer magnetic circuit is split into three sections to provide control of the current supplied to the thruster's outer magnetic coil circuit. The outer magnetic circuit is divided such that two coils are independently operated (OC2 and OC3), and six coils are connected in series to be operated using a TDK Lambda GEN60-25 power supply (OC1). The inner coil magnetic circuit is operated independently a TDK Lambda GEN60-25 power supply. Figure 3 shows a schematic representation of the electrical setup for the solenoids. The coil nomenclature employed in this study is delineated as follows: OC2 denotes coil 2, OC3 denotes coil 3, and OC1 collectively denotes coils 1 and 4 through 8. Through the control of current supplied to the outer magnetic coil circuit, the magnetic field observed in the channel is locally modified, resulting in the

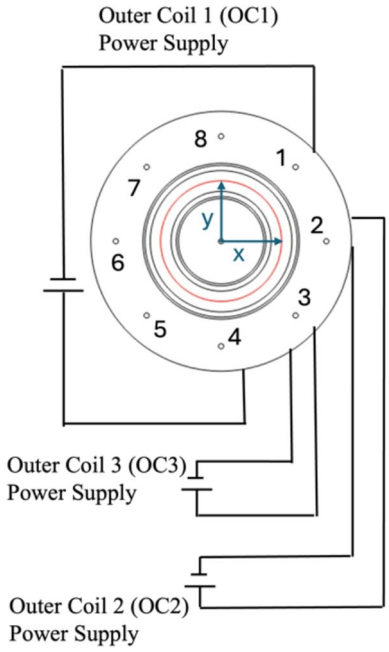

Fig. 3 Schematic of P5 electrical circuit for operation of the magnetic circuit solenoids

development of azimuthal magnetic field gradient causing plasma non-uniformities. The Cartesian coordinate system used in the current research considers horizontal sweep measurements at the centerline observed in xz plane with sweep direction as x and vertical sweep measurements at the centerline observed in yz plane with sweep direction as y with respect to the thruster.

Hemispherical sweep apparatus

The aluminum track hemispherical apparatus has a 1 m radius and is powered by a stepper motor with a step size of 1.8° per rotation. A stepper motor is employed in conjunction with limit switches positioned at the endpoints to monitor the probe's location as it moves along a curved path. The Ni motion controller MID-7604/7602 allows for the adjustment of the motor's speed during operation. At -45° and 50° from the track, high-precision limit switches are arranged so that the probe mount contact can activate the limit switch circuit and halt the motion of the probe. Figure 4 illustrates the conventional Faraday probe's standard horizontal trajectory sweep by red and the vertical sweep conducted using the sweep probe apparatus by green. The entire sweep probe apparatus is positioned on a radial probe arm so that there is a constant 1 m distance between the probe collector face and the thruster exit plane in VTF-2, as seen in Fig. 5. A laser alignment technique was conducted to precisely determine the angular orientation of the diagnostic probe in relation to the thruster centerline. The alignment technique guaranteed that the probe's position could be reliably referenced against both the thruster axis and a standard Faraday probe affixed to the radial arm at the thruster centerline. In this procedure, the laser delineated a straight line down the centerline of the thruster exit plane, and the probe assembly was calibrated until its angular orientation aligned with the established reference. The resultant angular coordinates were meticulously documented and subsequently included into the motion control software to provide consistent positioning and scanning throughout data acquisition. K-type thermocouple was

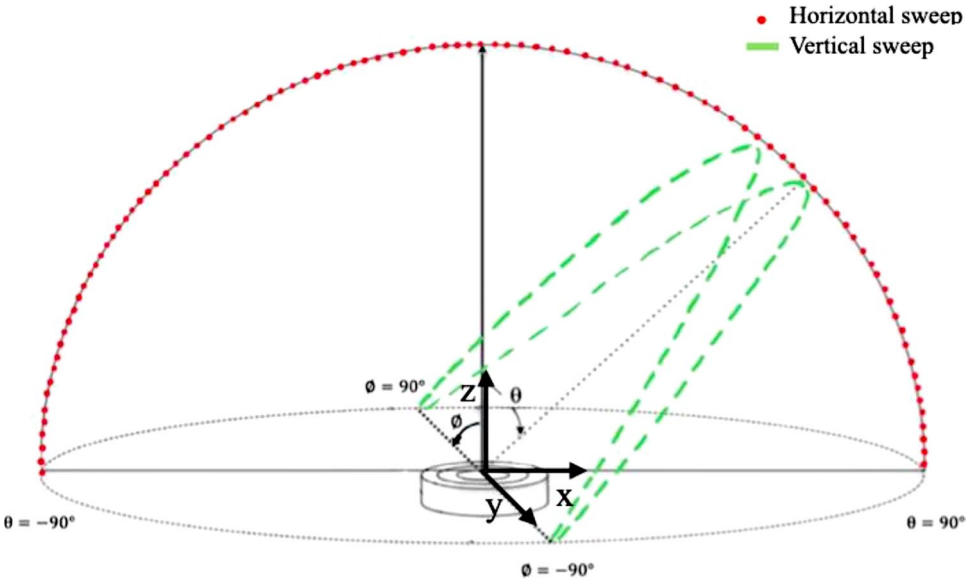

Fig. 4 Schematic of Faraday probe sweep path for the sweep probe apparatus

positioned at center the aluminum track to observe heating effects due to plasma plume. It was observed during the complete sweep that temperature fluctuations remained below 5° C as the probe traversed the plume, demonstrating a negligible heating effect on the probe. The effect of thermal expansion on the probe position was inconsequential for the scope of the current study thereby not compromising the accuracy of the measurements for the thrust vector. Further study would be required to observe heating effects across various positions on the track to guide better understanding of plume edge effects.

The radial probe arm is designed to undergo a horizontal sweeping motion, starting from – 90° and ending at 90° with a velocity of 0.63° per second. The probe arm is controlled using a Parker Daedal 200RT series rotary table, which has an accuracy of ± 0.17° [30], as depicted in Fig. 5b). The angular transverse motion and the stepper motor-driven vertical motion of the Faraday probe are controlled by Agilent 34970 A Data Acquisition Unit (DAQ). The Faraday probe's collector and guard ring are biased at -30 V relative to the ground using a Keithley 2470 Source meter. LabVIEW Virtual Instrument is used to record both the probe location and the ion beam current gathered by the Faraday probe on the sweep probe apparatus as well as the Faraday probe on the radial motion arm. Faraday probe mounted on the radial arm conducting horizonal sweep will be referred to as the conventional Faraday probe for the remaining of the paper. Calibration of the sweep probe apparatus was done with respect to the data obtained using the conventional Faraday probe setup deployed on the radial motion arm. Since the Faraday probe design was not modified, the results obtained using the two setups provided the consistency checks. Operation of the sweep probe apparatus in only horizontal scan configuration was the operation point to be used for the comparison and calibration of the setup in terms of electrical connections, probe design, operation etc.

Test conditions

The P5 thruster is powered by a voltage of 300 V, with the outer coil circuits (OC1, OC2, and OC3) and inner coil current set to 4 A and 6 A, respectively. The thruster runs

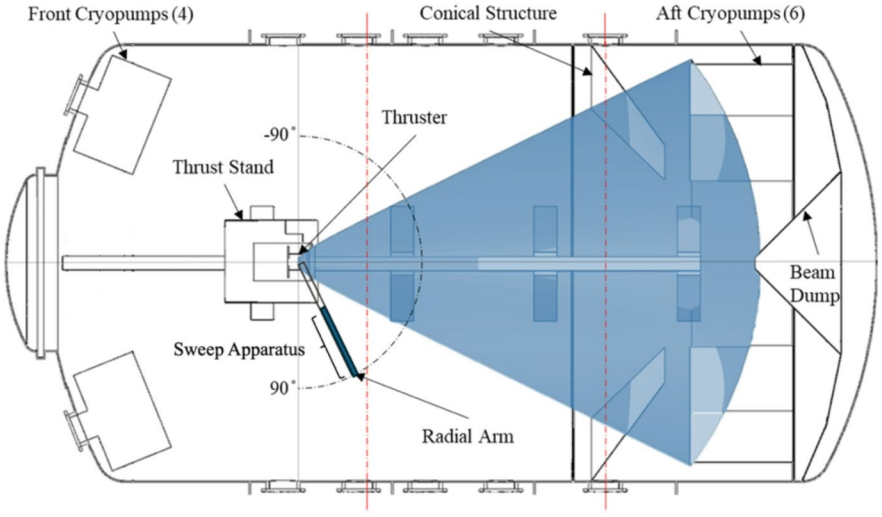

a)

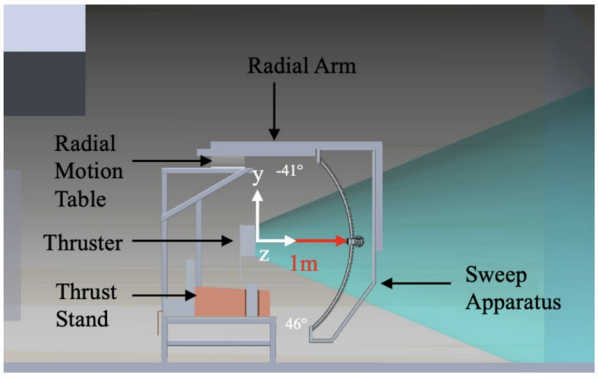

b)

Fig. 5 (**a**) and (**b**) Schematic orientation of the Sweep probe apparatus with respect to P5 in the VTF-2 chamber

for three hours before reaching a thermal steady state displayed by a rate of change of thruster temperature of less than 0.5 °C/min. After the thruster reaches a thermal steady state, a conventional Faraday probe mounted on the radial arm is utilized to take ion beam current measurements with a horizontal sweep from – 90° to 90° for comparison of ion beam current obtained through the measurements taken with the sweep probe apparatus with both horizontal (-90° to 90°)and vertical sweep(-41° to 46°) configuration. The guard and collector of the Faraday probe are biased at -30 V based on the recommended practices [22].

While taking three-dimensional measurements using hemispherical apparatus, three successive angular vertical sweeps of the Faraday probe from – 41° to 46° were done while measuring with sweep apparatus to remove motion control system error. The Faraday probe was scanned vertically from – 41° to + 46°, then returned from + 46° to – 41° and subsequently scanned again from – 41° to + 46°. The resultant scans displayed no noticeable variances or temporal delays, indicating the measurements' reproducibility. To further reduce any errors related to the motion control system (e.g., backlash, positioning offsets, or probe movement jitter), the vertical scan was conducted three times, and the resultant data sets were cross analyzed. This approach validated the precision

and uniformity of the assessed ion current density distribution. Following three vertical sweeps with the sweep apparatus, the probe arm is repositioned in a radial direction to conduct a vertical scan at the next horizontal position. Measurements are collected at intervals of 5° in the horizontal direction in the main plume, near the centerline. It takes two hours to perform the mapping of the entire plume region.

The collected data is subsequently analyzed utilizing the correction factors for charge exchange collisions (CEX) and analysis methodologies outlined by Brown [31]. The method mentioned has an error of around 5% for the beam current and 1.5% for the plume divergence half-angle [22, 32]. Characterization of ion beam current for uniform magnetic field configuration provides the baseline condition for comparison to analyze the effect of the magnetic field non-uniformities.

After the first testing configuration of uniform magnetic field, the second test condition involves the reduction of the current supplied to magnetic circuit OC2 to 0 A. The current reduction results in the introduction of a peak azimuthal magnetic field gradient of 0.31 G/° in the channel when measured using a FW Bell Gaussmeter 5080 before pump down. The magnetic field measurements are conducted near the exit plane where the peak of magnetic field is observed. The ion beam is characterized using the sweep probe apparatus at this non-uniform magnetic field condition to quantify the relationship between the magnetic field gradient and ion beam current as well as the thrust vector position. An increase in the magnetic field gradient is introduced through the reduction of current supplied to both OC2 and OC3 circuits to 0 A. An azimuthal gradient of 0.36 G/° is obtained in the operating condition. At this test condition, only the six coils connected in series are operational in the outer magnetic circuit, thus making this an extreme operating condition for the current study to evaluate the changes in thruster plasma characteristics using the developed diagnostic apparatus. At all the test conditions, Langmuir and RPA probes mounted on radial arm are utilized to provide measurements of electron temperature, plasma potential, and ion energy distribution function used to quantify plasma parameters at the centerline. Measurements of plasma parameters at the centerline allow for understanding variations in far-field plume properties due to non-uniformities in the channel.

In order to visualize the potential changes in the magnetic field in the presence of azimuthal magnetic field gradient, the variation in the magnetic field topology was visible in the COMSOL simulation for the two extreme conditions. The COMSOS simulation was executed with an import tolerance of 10^{-5}. The computational domain was delineated as a cylindrical border representing air, having a radius and height of 25 inches each. Material attributes were allocated to the thruster components based on their physical composition: copper, stainless steel, cast iron, and boron nitride. Mesh refining was user-directed, featuring an “extra fine” mesh option and a minimum element size of 0.0425 inches. A free tetrahedral meshing method was utilized in the boundary region, achieving convergence after four iterations. The coil geometry was examined utilizing physics-controlled modeling parameters, with the physics interface specified as the magnetic field module. This facilitated the assessment of the magnetic field distribution under authentic operational conditions.

The three-dimensional COMSOL simulation was conducted, with a two-dimensional slice obtained from the area of maximum magnetic field gradient, as illustrated in Fig. 6. The azimuthal magnetic field gradient is quantified in the text, increasing from 0.31.G/°

under the one-coil-off condition to 0.36 G/° when both coils are deactivated. Figure 6 demonstrates that the resultant field distribution has a pronounced inclination towards the outer coil, aligning with the noted augmentation in azimuthal gradient. As shown in Fig. 6, the change in the magnetic field line generates a deviation in the equipotential lines. The left side of the cross - section of the thruster displays the side of the thruster whether magnetic field gradient is introduced. The plot demonstrates the magnetic field lines along with the direction passing through the inner and outer coils closing the magnetic field circuit. Comparing the left side to the right side of thruster cross section, change in the magnitude as well as the variation in the direction of the lines is fairy visible. The magnitude of the deviation is contingent upon the span/length of the gradient and the magnitude of the magnetic field. Since magnetic field lines cannot be quantified in reality, the COMSOL simulations provide a good visualization tool for the magnetic fields present in the thruster at the extreme test conditions.

Results

This section examines the findings of operating the P5 thruster under non-uniform magnetic field conditions, specifically in the presence of an azimuthal magnetic field gradient. The ion beam current density measurements acquired by the Faraday probe on the sweep probe apparatus allowing three dimensional measurements are compared with those from the conventional Faraday probe configuration on the radial arm conducting a horizontal sweep on the centerline. As stated in previous section, the sweep probe apparatus provides a measurement span of 87 ° of the plume from – 41 to 46 ° vertically, due to the facility spatial restriction of VTF-2 while sweeping horizontally from – 90 to 90°. In order to estimate the ion beam current densities at the extremities in the vertical direction, it is assumed that the ion beam current density at the extremities is uniform three dimensionally. Thus, the vertical measurements spanning from 46 to 90° and – 41 to-90° are estimated via extrapolation using the horizontal measurements at 90 and – 90°.

The thrust vector traditionally is assumed to be estimated using the Gaussian distribution fit of the ion flux density data in the presence of twin peak [14]. Benavides at NASA Glen investigated thrust vector requirement for the Advanced Electric Propulsion System (AEPS) Hall-effect thruster using ion current density measurement using Faraday probes and demonstrated strong relationship with the beam centroid and the

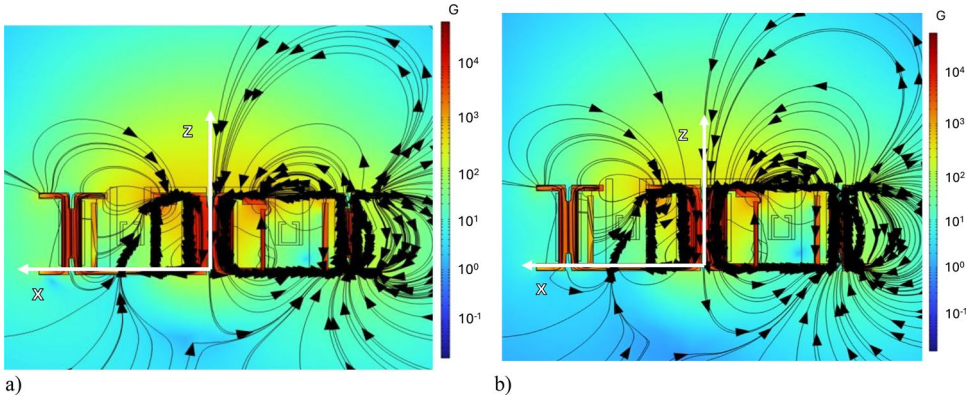

Fig. 6 COMSOL simulations of P5 magnetic field at (**a**) one coil off condition and (**b**) two coils off condition showing tilt towards the outer coil with an increase in azimuthal gradient

thrust vector [14]. The thruster vector position is estimated by measuring the centroid of the ion beam current density and normalizing the contribution of the ion flux. Though, the thrust vector is not directly measured with this approach, but a strong correlation to the behavior of the beam current density centroid and thrust vector is established. The study demonstrates weighted contribution of the beam current density to the thrust vector. The study observed the weight of ion flux at 6° to be the highest and the beam center to be the least. However, it is emphasized that despite the highest contribution in those areas, the resultant thruster vector is estimated based on the location of the resultant thrust vectors and hence the location of the centroid of the beam is important parameter for thrust vector orientation. Gaussian fit of the ion beam current density helps in estimation of beam centroid and was used to track the thrust vector orientation. The current research follows the same approach for estimation of thrust vector orientation based on ion current density measurements. A gaussian fit was performed on the measurement of ion beam current from − 41° to 46° in the current operation with absence of the twin peaks ensuring an R_{sq} value of minimum of 0.98. Despite the uncertainty associated with estimation of thrust vector measurement using the current approach, it provides indirect measurement technique for different thruster operations as well as a comparative estimation of the thrust vector orientation.

The P5 HET, operating at a voltage of 300 V on krypton with uniform magnetic field of 145 G, with an anode flow rate of 5.61 mg/s and a cathode flow rate of 0.44 mg/s, generated a discharge current of 7.9 A, resulting in an operational power of 2.3 kW. The standard setup for a Faraday probe involves attaching it to a radial arm and performing a horizontal sweep across the plume, covering an angle range from − 90° to 90°. After three successive scans for repeatability, the plume's horizontal sweep shows an ion beam current of 4.11 A and a divergence half angle of 33.2° for the P5 at 2.3-kW condition. The methodology specified by Brown [22] was followed to apply corrections for secondary electron emission (SEE) based on the material yield, ion current fraction and charge exchange (CEX) losses, which were substantiated by comparable literature values. The computed ion beam current incorporates the necessary adjustments for secondary electron emissions K_{SEE} and probe construction and is expressed as 95% of the total ion beam current The traditional method [22] relies on numerous assumptions, along with the assumption of the axisymmetric plume, to obtain total ion beam current I_b, axial ion beam current, I_a and divergence angle, λ. The total and axial ion beam current are used to calculate the charge flux weighted divergence angle for the far field plume as shown by Eqs. 2 and 3 where α_A is a piecewise function used to calculate plume divergence [22]. Nevertheless, this method is deemed inapplicable for operating conditions that exhibit unsymmetric plume characteristics and unsymmetrical magnetic field conditions.

$$I_b = 2\,\pi\; R^2 \int_0^{\pi/2} \frac{j\,[\theta\,]\,K_D}{K_A} sin\,(\theta\,)\,d\theta \tag{2}$$

$$I_a = 2\,\pi\; R^2 \int_0^{\pi/2} \frac{j\,[\theta\,]\,K_D}{K_A} cos\,(\alpha_A)\,sin\,(\theta\,)\,d\theta \tag{3}$$

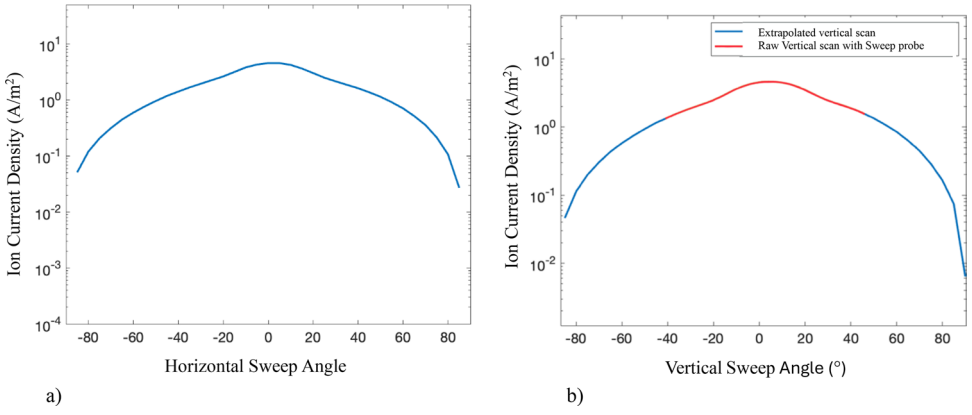

Fig. 7 (**a**) Ion current density as a function of horizontal sweep angle (**b**) extrapolated ion current as a function of vertical sweep angle at 300 V and 7.90 A with anode mass flow of 5.61 mg/s and cathode mass flow of 0.44 mg/s for uniform magnetic field condition using sweep probe apparatus

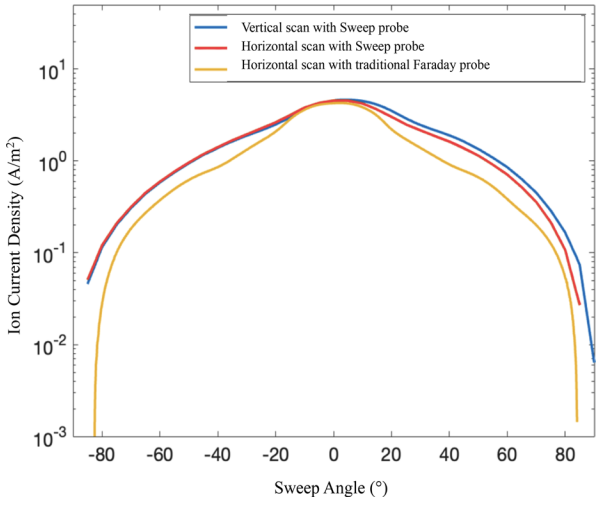

Fig. 8 Ion current density as a function of angle with (1) extrapolated vertical scan using sweep probe (2) horizontal sweep using sweep probe apparatus, (3) horizontal sweep using the traditional Faraday probe, apparatus for P5 operating at 300 V and 7.90 A with anode mass flow of 5.61 mg/s and cathode mass flow of 0.44 mg/s at uniform magnetic field condition

$$\lambda = cos^{-1}\left(\frac{I_a}{I_b}\right) \tag{4}$$

An examination of variations in plume behavior is conducted by performing a vertical sweep down the centerline using the sweep probe apparatus, with the horizontal position fixed at 0° and a horizontal sweep with the vertical position of probe fixed at 0°. The vertical sweep ranged from − 41° to 46° and is further extrapolated, as depicted in Fig. 7.

Figure 8 shows the ion beam current densities obtained with a typical Faraday probe setup on a probe arm [33] and the sweep probe apparatus to comprehend the extent of variations in the measurements. As illustrated in Fig. 7, the extrapolated vertical scan adhered to the trend of ion current density variation with sweep angles similar to the horizontal scan. The ion beam current fraction from the vertical scan is calculated to be 6.11 A after extrapolation, with a divergence angle of 35.3°. The analysis of the ion beam currents during horizontal and vertical scans revealed a 6% rise in ion beam current.

Faraday probes employed in the conventional horizontal configuration on motion arm and on the hemispherical sweep apparatus were identical in design with small differences due to manufacturing tolerances resulting in variations in measurements. The asymmetrical plume was initially attributed to the externally located cathode used to operate the P5. However, additional measurements with a centrally mounted cathode in future would provide further insight into the cause of the variation in the plume measurements. The discrepancies in ion beam current calculations necessitated using a three-dimensional mapping technique to obtain more precise plasma characteristics and plume asymmetry measurements.

The hemispherical sweep probe apparatus performed observations with a horizontal separation of 5° while scanning vertically from − 41° to 46° to obtain three-dimensional ion current measurements. The measurement uncertainty of the Faraday probe system was assessed by evaluating all pertinent error sources and aggregating them through a root-sum-square (RSS) method. The primary contribution originated from the probe, which had a ± 10% margin of error related to current collecting precision, electronic noise floor, and calibration tolerance. Laser alignment system is used to establish the centerline of the thruster and the corresponding position on the sweep probe apparatus is established. The Faraday probe is alignment with the centerline to establish 0° in vertical sweep position. The motion control system is used to set the coordinates for the vertical position of the Faraday probe at the centerline and the ends points. Corresponding step counts obtained using the motion controller for the centerline and the end points are recorded to keep track of position and establish accuracy. Multiple sweeps are taken to observe displacement of steps considering the error associated with the motion control system. A margin of error of less than ± 1% associated with the gear motion control system for vertical scan and a ± 2% for the horizontal motion control system. The variability between successive sweeps was assessed, and the corresponding uncertainty was integrated into the analysis to accommodate minor displacements or data correction artifacts. The application of this propagation method produced a combined uncertainty that resulted in a standard error aligning of 1.8×10^{-7} A/cm^2 associated with the three consecutive scans using the hemispherical sweep probe. While conducting vertical scans at various horizontal positions, ion current scans at the extremities, namely − 90° and 90° horizontal positions, diverged significantly from the trends found at the centerline. The ion current at the two extreme locations exhibited a linear variation with the angular sweep, as illustrated in Fig. 9. The examination of the facility depicted in Fig. 2 allowed for the assessment of the presence of propellant lines at the 90° angle horizontal position, as well as the metallic thrust structure at both locations, as a potential cause for the higher electrical currents observed at the wings compared to the center during a vertical scan. Though the measurements at the extremities are 100 times less in magnitude compared to the center of the thruster resulting in negligible contribution in magnitude of ion flux density. However, the variations at the extremities depict the impact of structural components located close to the thruster on the plume. The sweep probe apparatus is the sole effective tool for observing these effects and providing findings for future research.

Figure 10 presents the full 3-dimensional ion current density map. Equations 2, 3 and 4 have been modified to Eqs. 5, 6 and 6 in order to estimate the total ion beam current and beam divergence using the data obtained by the three-dimensional measurement

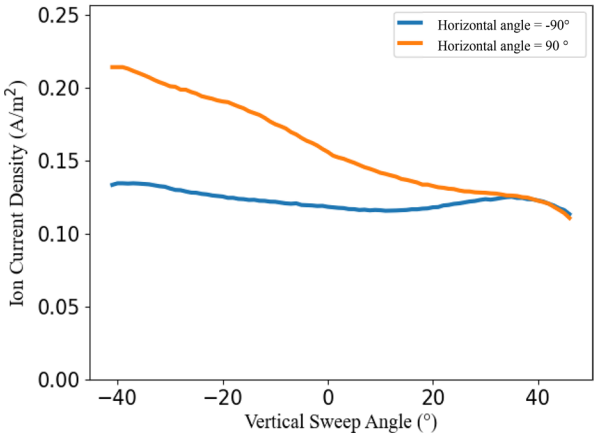

Fig. 9 Measured ion current density as a function of angle for vertical scan at -90° and 90° horizontal position

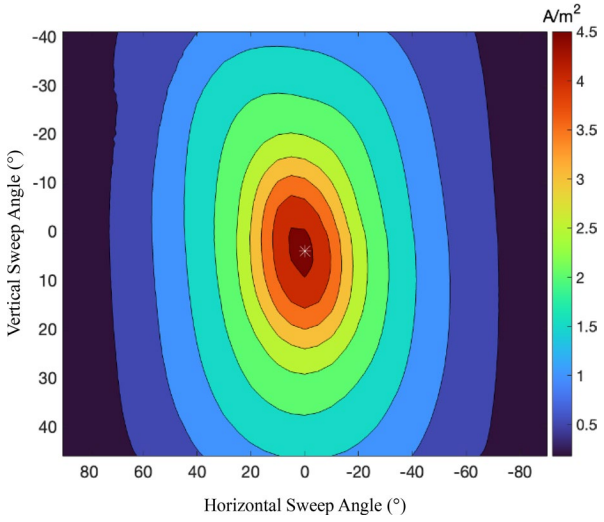

Fig. 10 Contour map of ion current density with horizontal and vertical sweep angle depicting the position of the plume center for baseline condition

technique. The analysis of the raw data from the three-dimensional sweep yielded an estimated ion beam current of 3.60 A, accompanied by a divergence angle of 26.0° for − 41° to + 46° instead of -90° to 90° in the vertical direction. The data is corrected for secondary electron emission and charge exchange only in the horizontal direction, as the vertical sweep is restricted to -41° to 46°. The hemispherical scan yielded a 36.9% decrease in the measurement of ion beam current due to the restricted vertical sweep range. The vertical scans were extrapolated using the horizontal scan measurements to determine the potential full-scale measurement of the ion beam current while preserving the trend of ion current density variation across the 37 vertical scans. The methodology presumes that the far-field ion beam at elevated vertical angles displays minimal azimuthal asymmetry. Assuming this, the vertical attenuation of current density at the boundaries can be depicted using scaling profiles derived from the outermost observed vertical positions (− 41° and + 46°). The current density distribution obtained at the horizontal extremities (± 90°) served as a reference shape for the extrapolated vertical regions, scaled to provide smooth value continuity at the boundary angles of − 41° and

+46°. This guaranteed the consistency of the current density profile during the shift from measured to extrapolated data. The data extrapolation resulted in measurements that span from −90° to 90° in both the vertical and horizontal directions, thereby enabling the total estimation of the hemispherical ion current for P5 at 2.3 kW, as illustrated in Fig. 11.

$$I_{b\_3d} = R^2 \int_{-\pi/2}^{\pi/2} \int_{-\pi/2}^{\pi/2} \frac{j\,[\theta\,,\varnothing\,]\,K_D}{K_A} sin\,(\theta\,)\,d\theta\,d\varnothing \tag{5}$$

$$I_{a\_3d} = R^2 \int_{-\pi/2}^{\pi/2} \int_{-\pi/2}^{\pi/2} \frac{j\,[\theta\,,\varnothing\,]\,K_D}{K_A} cos\left(\alpha_{A\_3d}\right) sin\,(\theta\,)\,d\theta\,d\varnothing \tag{6}$$

$$\lambda_{3d} = cos^{-1}\left(\frac{I_{a\_3d}}{I_{b\_3d}}\right) \tag{7}$$

An ion beam current measurement of 5.71 A and a divergence angle of 33.9° is obtained from the extrapolated three-dimensional ion current by using Eqs. 5–7. The ion beam current measurements were evaluated after correcting for secondary electron emission and charge exchange at horizontal and vertical angles, yielding a 95% ion beam percentage. The hemispherical sweep mechanism had a negligible effect on the floating potential of the thruster, keeping it constant at -5.84 V and allowing it to be used without impacting its operation. The floating potential consistently measured at – 5.84 V within the measurement system's resolution, signifying that the sweeping motion did not disturb the thruster plasma or cause additional variations. A direct comparison to a case without the apparatus was not conducted; nonetheless, it is seen that the probe arm assembly was electrically isolated and enough distanced to reduce plume disruption. The measurements acquired with the hemispherical apparatus were subject to uncertainty. This uncertainty included a ± 10% margin of error connected with the Faraday probe [22] and a margin of error of less than ± 1% associated with the gear motion control system for vertical scan and a ± 2% for the horizontal motion control system.

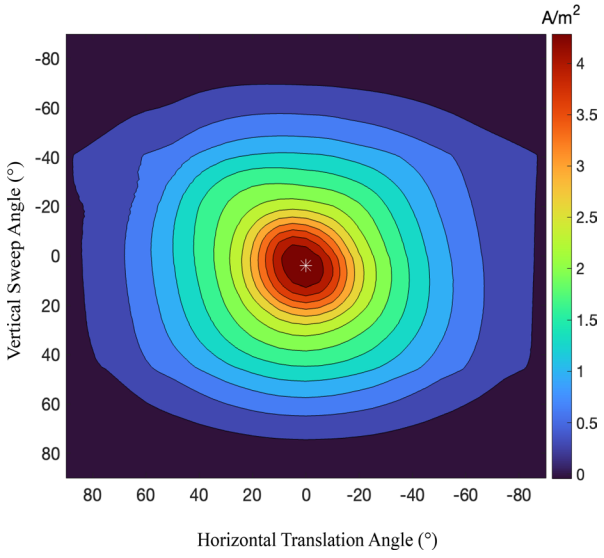

Fig. 11 Contour map of ion current density with horizontal and vertical sweep angle containing extrapolated measurements depicting the position of the plume center for baseline condition

The horizontal scan is conducted using the sweep apparatus when the magnetic circuit 2 (OC2) is powered off, which yielded a 95% ion beam fraction of 4.33 A and a half divergence angle of 34°. The extrapolated vertical scan for the test condition resulted in an ion beam current fraction of 4.74 A, with a divergence angle of 34°. The analysis of the ion beam currents during horizontal and vertical scans revealed a 9.5% rise in ion beam current. Ion current collected through the complete three-dimensional mapping for this operating condition after extrapolation to -90 to 90 is illustrated in Fig. 12.

The analysis of the raw data from the three-dimensional sweep yields an estimated ion beam current of 2.24 A, accompanied by a divergence angle of 26°. The total extrapolated ion beam current for P5 at 2.3 kW with OC2 circuit off resulted in a magnetic field gradient of 0.31 G/,ion beam current measurement of 4.40 A and a divergence angle of 34°. The ion beam current measurements are evaluated after correcting for secondary electron emission and charge exchange at horizontal and vertical angles, yielding a 95% ion beam percentage.

The horizontal scan conducted using the sweep apparatus when magnetic circuits 2 and 3 (OC2 and OC3) were powered off yielded a 95% ion beam fraction of 4.26 A and a half divergence angle of 34°. The extrapolated vertical scan for the test condition resulted in a 95% ion beam current fraction of 4.59 A, with a divergence angle of 34°. The analysis of the ion beam currents during horizontal and vertical scans revealed a 7.7% rise in ion beam current. Ion current collected through the complete three-dimensional mapping for this operating condition after extrapolation to -90 to 90 is illustrated in Fig. 13.

The analysis of the raw data from the three-dimensional sweep yielded an estimated ion beam current of 2.19 A, accompanied by a divergence angle of 26°. The total extrapolated ion beam current for P5 at 2.3 kW with OC2 and OC3 circuit off resulted in a magnetic field gradient of 0.36 G/° ,ion beam current measurement of 4.33 A and a divergence angle of 34°. The ion beam current measurements were evaluated after correcting for secondary electron emission and charge exchange at horizontal and vertical angles, yielding a 95% ion beam percentage. A deviation in the thrust vector in the vertical direction was detected for uniform and non-uniform test conditions using the

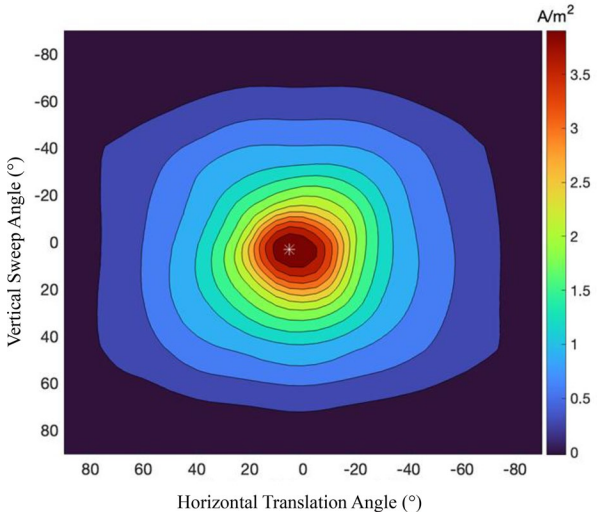

Fig. 12 Contour map of ion current density with horizontal and vertical sweep angle containing extrapolated measurements depicting the position of the plume center for one coil-off configuration

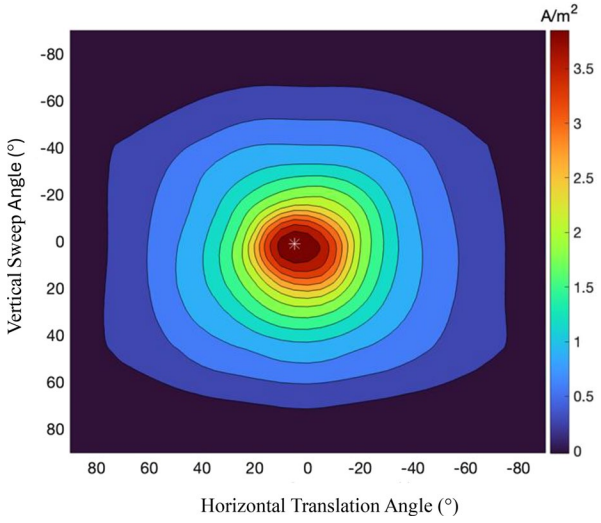

Fig. 13 Contour map of ion current density with horizontal and vertical sweep angle containing extrapolated measurements depicting the position of the plume center for two coils off configuration

measurements obtained from the sweep probe apparatus. This deviation in the thrust vector could not be obtained using the standard Faraday probe horizontal sweep.

Discussion

This section examines the effects of azimuthal magnetic field gradients on ionization and acceleration processes within the thruster channel, elucidating the influence of magnetic field non-uniformities on thrust vector orientation. The experimental results acquired from the sweep probe device, which facilitates three-dimensional plume mapping, yield more precise measurements due to enhanced measurement space capabilities. The sweep probe device enhances thruster vectoring measuring capabilities by quantifying centroid of ion beam current densities that reflect fluctuations in thruster vectoring as an azimuthal magnetic field gradient is applied within the channel. The three-dimensional plume mapping, obtained using the developed apparatus, establishes a foundation for further investigation of thruster performance under non-uniform magnetic fields.

Measurements of ion beam current at uniform and non-uniform magnetic field conditions demonstrate the impact of the magnetic field on the plasma ion beam. The ion beam current is estimated using the ion current density measurements collected by the sweep of the Faraday probe, as shown in Eq. 1. The horizontal and vertical Faraday probe sweeps at centerline using the sweep probe apparatus provide the measurements for ion beam current and beam divergence for the three test conditions, as seen in Table 1. A 9.6% decrease in the local magnetic field demonstrated a 24% reduction in the ion beam current when measurements were conducted using the traditional horizontal sweep. In contrast, a 22% reduction in ion beam current and a 2.8% reduction in the divergence of the ion beam is recorded for vertical scans when moved from uniform to non-uniform magnetic field configuration. A 16.5% decrease in the local magnetic field demonstrated a 25% reduction in the ion beam current when measurements were conducted using the traditional horizontal sweep. In contrast, a 25% reduction in ion beam current and 2.8% in reduction divergence of the ion beam is observed for vertical scans at the extreme operating condition. The variations in the ion beam current change with the magnetic field as the sweep direction for measurement is varied, provides proof of

Table 1 Horizontal and vertical sweep measurements of ion beam current and beam divergence at uniform and non-uniform operating configurations at 300 V, 5.61 mg/s anode, and 0.44 mg/s cathode flow rates using sweep probe apparatus at centerline configuration

Test Condition	Sweep probe apparatus Configuration at centerline	Ion beam Current (A)	Half Divergence Angle (°)
Uniform -baseline	Horizontal Sweep	5.71	35
OC2 circuit off- one coil off	Horizontal Sweep	4.33	34
OC2 and OC3 circuit off- two coils off	Horizontal Sweep	4.26	34
Uniform -baseline	Vertical Sweep with extrapolation	6.10	35
OC2 circuit off- one coil off	Vertical Sweep with extrapolation	4.74	34
OC2 and OC3 circuit off- two coils off	Vertical Sweep with extrapolation	4.59	34

Table 2 Extrapolated three-dimensional sweep measurements of ion beam current and beam divergence at uniform and non-uniform operating configurations at 300 V, 5.61 mg/s anode, and 0.44 mg/s cathode flow rates using sweep probe apparatus

Test condition	B_l (G)	Ion beam Current (A)	Half Divergence Angle (°)
Uniform -baseline	145	5.71	35
OC2 circuit off- one coil off	131	4.40	34
OC2 and OC3 circuit off- two coils off	121	4.33	34

the non-symmetric nature of plume. Hence, it is essential to perform a complete three-dimensional mapping of the ion beam to observe changes with non-uniformities present in the thruster.

Table 2 provides measurements obtained from the three-dimensional sweeping of the Faraday probe, highlighting a 16.5% decrease in the local magnetic field, resulting in a 24% decrease in ion beam current and a 2.8% decrease in divergence angle when the magnetic field is varied from uniform to non-uniform. The decrease in beam divergence is lower than the decrease in ion beam current as the ion beam divergence is a function of axial electric field and plasma potential distribution near the channel exit. As the local magnetic field decreases by 16.5% resulting in decrease in electron confinement and ionization rate, leading to 24% decrease in ion beam current, the axial electric field and radial plasma potential distribution is largely unaffected. Quasi-neutrality of the plasma ensures that the radial electric fields remain nearly unchanged, and the channel geometry sets the baseline ion trajectories. Thus, the ratio of radial to axial ion velocities, which governs the beam divergence angle, is only observing a decrease of 2.8% and minimally affected. The total uncertainty in the measured ion current density using the Hemispherical sweep apparatus is obtained by propagating all independent error sources using a root-sum-square (RSS) formulation:

$$\left(\frac{\delta J}{J}\right)^2 = \left(\frac{\delta I}{I}\right)^2 + \left(\frac{\delta A}{A}\right)^2 + \left(\frac{\delta J_{\text{geom}}}{J}\right)^2 + \left(\frac{\delta J_{\text{sheath}}}{J}\right)^2 \tag{8}$$

where $\frac{\delta I}{I}$ represents the error associated with ion current collection using the Faraday probe, $\frac{\delta A}{A}$ represents the error associated with the effective collection area of the probe, $\frac{\delta J_{\text{geom}}}{J}$ represents the error associated with mechanical components as well as the angular resolution capability of the apparatus and $\frac{\delta J_{\text{sheath}}}{J}$ represent the plasma sheath effects and interactions with the collection probe which in the current design is the Faraday Probe. As stated previously, the dominant uncertainty of 10% in the collected ion

current arises from probe electronics, calibration tolerance, and current collection efficiency associated with the Faraday probe. The manufacturing tolerances and alignment of the probe introduces 3–5% uncertainty in the effective collection area of the probe. Due to the same probe being utilized for all scans, this uncertainty is systematic and does not affect the relative comparison between different operating conditions. Combining the error associated with both the horizontal and vertical motion control system

$$J_{\text{geom}} \approx \left| \frac{\partial J}{\partial \theta} \right| \delta\theta + \left| \frac{\partial J}{\partial \varphi} \right| \delta\varphi \tag{9}$$

The total uncertainty associated with the position accuracy is 3%. Using measured angular gradients from repeated sweeps, this contribution was quantified experimentally confirming the mechanical displacement errors remain sub-dominant relative to probe current uncertainty. Operating in limited sheath impact conditions, the total uncertainty contributions using RSS:

$$\frac{\delta J_{\text{total}}}{J} \approx 13\%$$

Thus, the total uncertainty in absolute ion current density measured using the hemispherical sweep probe apparatus is approximately ± 10–15%, consistent with values reported in comparable Faraday probe diagnostics. The total uncertainty in beam divergence is obtained by propagating uncertainties in current density and angular position for both angles. The uncertainty associated with the current density for the current design is 13%.

$$\delta\lambda_{3d}^2 = \left(\frac{\partial\lambda_{3d}}{\partial\theta}\delta\theta\right)^2 + \left(\frac{\partial\lambda_{3d}}{\partial\phi}\delta\phi\right)^2 \tag{10}$$

Although the Faraday probe introduces an estimated ± 10% uncertainty in absolute ion current density, beam divergence is derived from normalized angular moments of the current distribution. As a result, multiplicative probe uncertainties cancel analytically, leaving divergence sensitive only to angular non-uniformities in probe response and positioning, which contribute an effective uncertainty of approximately 1–2%. Through the repeated hemispherical scans, a $\pm 0.9^\circ$ scan to scan standard deviation was observed. The study was performed with the hemispherical sweep apparatus being operated at horizontal sweeping intervals 5°. Due to the magnetic field change being present in a relatively smaller localized area, making it challenging to observe beam divergences in the said operating condition of the hemispherical sweep apparatus. Thus, the total error associated with the hemispherical sweep probe apparatus while obtaining beam divergence require future studies. In order obtain more accurate results and characterize the sweep probe apparatus, future work will be performed with final resolution for the horizontal sweeping angle to characterize the angular positioning errors associated with beam divergence.

To understand the impact of non-uniformities in magnetic field on ion beam current, it is essential to understand the effect on the ionization and acceleration processes. The current study involves the introduction of an azimuthal magnetic field gradient due to the localized region's loss of magnetic field. The electron's confinement in the channel decreases as the electrons transition from the high uniform magnetic field region to a

lower magnetic field sectional region as a result of the gradient's introduction in the HET channel. The lesser confinement of the electrons is bound to increase the electron flux in the gradient region. The reduction in confinement would lead to a decrease in collision frequency, resulting in a decrease in ionization due to the reduced electron number density. Decrease in confinement of electrons would also cause less ohmic heating, leading to a decrease in temperature due to the decreased likelihood of ionization collisions. A decrease in the electron temperature would result in a decrease in the energy possessed by the charged species, which potentially results to a less positive plasma potential at that location. Therefore, an azimuthal magnetic field gradient in the non-uniform operating condition would result in a non-uniform distribution of the electron number density and electron temperature in the channel. The decrease in energy could cause the electrons to travel upstream in the region of the azimuthal gradient to gather energy for ionization. This motion would lead to a localized shift in the ionization acceleration region, causing the region to move upstream towards the anode at the gradient's location.

The length of the acceleration region, L_a is hypothesized to increase in the magnetic field gradient region due to the variations in the location of the ionization acceleration region. Consequently, the azimuthal gradient influences the ions, as they could now formed further upstream within the localized region. The loss voltage would increase as a result of the increased likelihood of wall collisions and neutralization collisions among the ions. The acceleration voltage decreases due to the increase in the loss voltage for a fixed discharge voltage. The decrease in acceleration voltage could indicate a reduction in ion velocity, which causes a decrease in the ion beam current, I_b. It is vital to note that an azimuthal magnetic field gradient influences plasma characteristics in the confined region and causes an overall reduction across the channel. The average integral of the energy distribution of the electron varies from the uniform magnetic field baseline condition as the electron transitions from the low magnetic field gradient region to the high magnetic field uniform region, resulting in reduced energy. The following equations are used to establish relationship between the measured properties and plasma parameters with the assumptions that in the acceleration region the electric field intensity and the radial magnetic field induction are constant [34].

$$I_b = \ n_i e v_i A \tag{11}$$

$$v_i = \sqrt{\frac{2eV_a}{m_p}} \tag{12}$$

$$\frac{V_d}{B_r^2 L_a b_c} = constant\ , \ \ L_a \propto \ \frac{1}{B_r} \tag{13}$$

The results presented emphasize the change in plasma parameters at the far field despite the azimuthal gradient, resulting in the highest reduction in the magnitude of the magnetic field, which is 16.5% of the baseline magnetic. The plasma properties obtained using Langmuir and RPA probes as shown in Table 3 provide proof of the proposed explanation for the effect of the magnetic field non-uniformities on the ion beam characteristics [35]. The experimental results demonstrated a reduction of 8.12% in electron temperature and a decrease of 5.09% in acceleration voltage compared to the baseline condition when one coil is turned off. Additionally, there is a decrease of 12.9% in

Table 3 Langmuir and RPA probe measurements for azimuthal magnetic field gradient test conditions at 300 V, 5.61 mg/s anode, and 0.44 mg/s cathode flow rates

Test condition	B_l (G)	T_e(eV)	$n_e(m^{-3})$	V_p(V)	V_{rpa} (V)
Uniform -baseline	145	4.3	2.0×10^{15}	14.9	269.8
OC2 circuit off- one coil off	131	3.9	1.9×10^{15}	14.6	256.5
OC2 and OC3 circuit off- two coils off	121	3.7	1.5×10^{15}	14.0	253.5

Table 4 Thrust vector position for azimuthal magnetic field gradient test conditions at 300 V, 5.61 mg/s anode, and 0.44 mg/s cathode flow rates

Test Condition	B_l (G)	$\nabla_\theta B_r$ (G/°)	Horizontal (°)	Vertical (°)
Uniform -baseline	145	0.00	0	4
OC2 circuit off- one coil off	131	0.31	5	3
OC2 and OC3 circuit off- two coils off	121	0.36	5	1

electron temperature and a reduction of 6.03% in acceleration voltage when two coils were turned off. Despite the good repeatability of measurement under fixed operating conditions, the systematic uncertainty associated with the Langmuir probe produces ± 10–20% variation in electron temperature and ± 10–30% variation in the electron density [25]. Similarly, the error associated with RPA stays within ± 10–20%, with repeatability of ion energy within ± 1–3% [36]. The dominant sources of RPA uncertainty arise from grid transparency, secondary electron emission from the grids, charge-exchange ion production in the plume, and local plasma-potential variation at the probe location. Examining the uncertainty linked to the Langmuir and RPA probe, there is a strong rationale for the capability to detect the impact of the azimuthal gradient on the plasma parameters [35].

The azimuthal magnetic field gradient influenced the thruster performance in terms of magnitude and the plume's orientation. The beam centroid's position is determined and tracked using three-dimensional plume mapping to predict the position of the thrust vector. Qualifying a thrust vector is an intricate process that requires indirect measuring techniques to quantify the attributes associated with the thrust vector accurately. Plasma properties, including the ion beam current, are estimated to determine the location of the thrust vector. As a result of the indirect measurement techniques, it is necessary to make assumptions regarding the orientation of thrust vector and ion beam current density as stated in previous section. It is presumed that the centroid of the ion beam current density provides estimation of thrust vector orientation. Consequently, the experiment is conducted in the absence of a double peak, thus using a Gaussian fit on the beam resulted in estimation of beam centroid. Table 4 displays the thrust vector's location for the baseline condition and the varying azimuthal magnetic field gradient condition. The thruster's inclination is measured during the installation process, and a vertically downward angular incline of 0.2° is determined. This inclination doesn't impact the thruster vector position obtained for the baseline condition and, as a result, is disregarded in the current analysis. The maximum value of the ion current is observed to occur at the center line of the thruster in the horizontal sweep direction, which is consistent with the horizontal sweep direction observed using the conventional Faraday probe device. The vertical scan, as well as the three-dimensional scan, offered an alternative representation of the position of the thrust vector. The plume center is located 4 degrees

below the center of the thruster. The capacity to provide high-resolution vertical scans with measurements taken at 0.1° intervals made such plume characterization possible and provided excellent tracking capabilities. The three-dimensional probe device offered additional validation for its potential application as a measurement tool for tracking the thrust vector of the HET plume. The two coils, independently actuated, were situated on the right side of the thruster when viewed from the front, as illustrated in Fig. 3. The position of the thrust vector changed to 5° horizontally and 3° vertically when the OC2 circuit is off. The incorporation of azimuthal gradient in the magnetic field leads to a reduction in the frequency of ionization collisions. Furthermore, the alteration in length within the ionization acceleration region causes a decrease in the overall ion beam current observed during the scan conducted with the sweep probe apparatus to measure ion current density. The ion current density centroid was deviated due to the magnetic field lines passing through the inner coil being modified due to the OC2 circuit being turned off and tilted towards the outer coil rather than at the centerline location, which was probable for the magnetic field lines. The OC2 and OC3 circuits being off corresponded to the two coils being turned off condition. It is evident that the presence of a 0.04 G/° higher gradient, as opposed to a single coil being off, caused a 2° vertical deviation in the thrust vector. The magnetic field experienced a greater magnitude decrease due to the additional coil's turning off. Additionally, the gradient was able to traverse a larger area, resulting in a fluctuation in the vertical position of the centroid.

The sweep apparatus offered significant benefits in accurately measuring thruster performance, identifying plume non-uniformities across horizontal and vertical, and tracking the thrust vector. The current study provided a reasonable estimation of the effects of azimuthal magnetic field gradient on the ion beam current and thrust vector. Thus, this apparatus can be utilized to test thrusters with vectoring capabilities and to examine the effects of clustering thrusters at different positions on the direction of the thruster vector. The sweep probe apparatus's potential utilization for ion current measurement at the points of non-uniformities in the plasma highlights the importance of the instrument and allows better quantification of the accuracy of the measurements. Future studies using Langmuir and RPA probe on the sweep apparatus can help in providing more knowledge of the variation of plasma parameters due to non-uniformities and allow better thrust vector measuring capabilities.

Conclusion

The hemispherical sweep probe apparatus equipped with a Faraday probe demonstrated the three-dimensional measurement of ion current across the HET distribution to get precise measurements of ion beam current for P5 HET operating with uniform and non-uniform magnetic field configurations. The apparatus allows the user to quantify non-uniformities in the plasma plume parameters and estimate the location of the thrust vector. The ion beam current measurements using sweep probe apparatus yielded close proximity to the ion beam current obtained by the horizontal sweep measurements. The mapping of the plume illustrates the importance of the hemispherical sweep equipment in obtaining greater precision in measurements of plume parameters without interfering with thruster operation. The thruster vector tracking capabilities of the sweep apparatus also enabled the quantification of the vertical asymmetry of the P5 HET plume, with an inclination of 4° while maintaining the horizontal symmetry. The sweep probe apparatus

allowed for observation of 0.36 G/° azimuthal magnetic field gradient resulting in 24% decrease in ion beam current and 5.8° spatial variation of the thrust vector. The potential of the three-dimensional sweep probe apparatus for observing thruster plume non-uniformities and tracking thrust vectors for HET and HET clusters opens new possibilities for future electric propulsion research.

Nomenclature

m_i	ion mass, kg
L_a	Length of accelerating channel, m
V_d	discharge voltage, V
V_a	accelerating voltage, V
e	electron charge, C
I_b	Ion beam current, A
n_i	ion number density, m^{-3}
v_i	average ion velocity, m s^{-1}
A	cross-sectional area of the discharge chamber, m^2
m_e	mass of electron, kg
j	electron current density, A m^{-2}
B_r	radial component of the magnetic field, T
θ	angular coordinate
B	magnitude of the magnetic field, T
K_D	correction for probe distance to thruster
K_A	correction for ion angle of incidence
b_c	channel width, mm
R	Radial measurement distance, m
B_l	maximum local magnetic field in the azimuthal gradient region, G
$\nabla_\theta B_r$	azimuthal magnetic field gradient, G/°

Author contributions

Conceptualization: Chhavi Chhavi and Mitchell L.R. Walker; literature search, diagnostic development and data analysis: Chhavi Chhavi; Writing—original draft preparation: Chhavi Chhavi; Writing -review and editing: Chhavi Chhavi and Mitchell L.R. Walker. The author(s) read and approved the final manuscript.

Funding

No funding used for this research.

Data availability

No datasets were generated or analysed during the current study.

Declarations

Competing interests

Mitchell Walker is an Editorial Board member of Journal of Electric Propulsion, and they were not involved in the journal's review of, or decisions related to, this manuscript.

Received: 26 May 2025 / Accepted: 21 January 2026

Published online: 28 January 2026

References

1. Jahn RG (2006) Physics of electric propulsion. Dover Publ, Mineola, NY
2. Goebel DM, Katz I (2008) Fundamentals of electric propulsion: ion and hall thrusters. Wiley. https://doi.org/10.1002/9780470436448
3. Hofer R, Gallimore A (2006) High-Specific impulse hall Thrusters, part 2: efficiency analysis. J Propuls Power - J PROPUL POWER 22:732–740. https://doi.org/10.2514/1.15954
4. O'Reilly D, Herdrich G, Kavanagh DF (2021) Electric propulsion methods for small satellites: A review. Aerospace 8(1):22. https://doi.org/10.3390/aerospace8010022
5. Lev D, Myers RM, Lemmer KM, Kolbeck J, Koizumi H, Polzin K (2019) The technological and commercial expansion of electric propulsion. Acta Astronaut 159:213–227. https://doi.org/10.1016/j.actaastro.2019.03.058
6. Bapat A, Salunkhe PB, Patil AV (2022) Hall-Effect thrusters for Deep-Space missions: A review. IEEE Trans Plasma Sci 50(2):189–202. https://doi.org/10.1109/TPS.2022.3143032
7. Raitses Y, Guelman M, Ashkenazy J, Appelbaum G (1999) Orbit transfer with a variable thrust hall thruster under drag. J Spacecr Rockets 36(6):875–881. https://doi.org/10.2514/2.3506
8. Misuri T, Pergola P, Andrenucci M (2013) HT5k Hall Thruster to Improve Small Launcher Capabilities, presented at the In Proc. 33rd International Electric Propulsion Conference
9. Jackson J, Cassady J, Allen M, Myers R, Tofil TA, Herman DA, Pencil EJ (2018) Development of High Power Hall Thruster Systems to Enable the NASA Exploration Vision, presented at the 2018 Space Propulsion Conference, Seville
10. Hofer RR (2004) Development and Characterization of High-Efficiency, High-Specific Impulse Xenon Hall Thrusters, Ph.D. Dissertation, University of Michigan

11. Reid BM, Gallimore A (2007) Review of Hall Thruster Neutral Flow Dynamics
12. Benavides GF, Kamhawi H, Liu TM, Pinero LR, Verhey TR, Rhodes CR, Yim JT, Mackey JA, Gray TG, Butler-Craig NI, Myers JL, Birchenough AG (2019) Development of a High-Propellant Throughput Small Spacecraft Electric Propulsion System to Enable Lower Cost NASA Science Missions, presented at the AIAA Propulsion and Energy Forum 2019, Indianapolis, IN, 2019
13. Lazurenko A, Kim V, Bishaev A, Auweter-Kurtz M (2005) Three-Dimensional simulation of atom and ion dynamics in a stationary plasma thruster. J Appl Phys 98(4):043303. https://doi.org/10.1063/1.2009821
14. Benavides GF, Mackey J, Ahern D, Thomas R (2018) Diagnostic for Verifying the Thrust Vector Requirement of the AEPS Hall-Effect Thruster and Comparison to the NEXT-C Thrust Vector Diagnostic, presented at the Joint Propulsion Conference, Cincinnati, Ohio, 2018. https://doi.org/10.2514/6.2018-4514
15. Sohl G, Fosnight VV (1969) Thrust vectoring of ion engines. J Spacecr Rockets 6(2):143–147. https://doi.org/10.2514/3.29552
16. HOMA J, WILBUR P (1982) Ion Beamlet Vectoring by Grid Translation, 16th International Electric Propulsion Conference, American Institute of Aeronautics and Astronautics. https://doi.org/10.2514/6.1982-1895
17. Van Reijen B, Weis S, Lazurenko A, Haderspeck J, Genovese A, Holtmann P, Ruf K, Püttmann N (2013) High precision thrust vector determination through full hemispherical RPA measurements assisted by angular mapping of ion energy charge state distribution
18. Pollard J, Welle R (1995) Thrust Vector Measurements with the T5 Ion Engine, 31st Joint Propulsion Conference and Exhibit, American Institute of Aeronautics and Astronautics. https://doi.org/10.2514/6.1995-2829
19. Polk J, Anderson J, Brophy J (1998) Behavior of the Thrust Vector in the NSTAR Ion Thruster, 34th AIAA/ASME/SAE/ASEE Joint Propulsion Conference and Exhibit, American Institute of Aeronautics and Astronautics. https://doi.org/10.2514/6.1998-3940
20. Haag T (2002) Translation Optics for 30 Cm Ion Engine Thrust Vector Control, IEPC-01-116
21. Gulczinski F, Examination of the structure and evolution of ion energy properties (1999) OF A 5 kW Class laboratory hall effect thruster at various operational conditions. Univ Mich
22. Brown DL, Walker MLR, Szabo J, Huang W, Foster JE (2017) Recommended practice for use of Faraday probes in electric propulsion testing. J Propul Power 33(3):582–613. https://doi.org/10.2514/1.B35696
23. Brown DL, Gallimore AD (2009) Evaluation of plume divergence and facility effects on far-field Faraday probe current density profiles, in the 31st International Electric Propulsion Conference (IEPC-2009-030)
24. Walker MLR, Hofer RR, Gallimore AD (2002) The effects of nude Faraday probe design and vacuum facility backpressure on the measured ion current density profile of Hall thruster plume, in Proceedings of the 38th AIAA/ASME/SAE/ASEE Joint Propulsion Conference and Exhibit. AIAA https://doi.org/10.2514/6.2002-4253
25. Walker MLR, Victor AL, Hofer RR, Gallimore AD (2005) Effect of backpressure on ion current density measurements in hall thruster Plumes. J Propul Power 21(3):408–415. https://doi.org/10.2514/1.7713
26. Kieckhafer AW (2011) Recirculating Liquid Nitrogen System for Operation of Cryogenic Pumps, presented at the 32nd International Electric Propulsion Conference, Electric Rocket Propulsion Society, Wiesbaden, Germany, IEPC-2011-217
27. Dushman S (1949) Scientific foundations of vacuum technique. J Wiley
28. Haas JM, Gallimore AD (2001) Internal plasma potential profiles in a Laboratory-Model hall thruster. Phys Plasmas 8(2):652–660. https://doi.org/10.1063/1.1338535
29. Peterson P, Gallimore A, Haas J (2001) Experimental Investigation of Hall Thruster Internal Magnetic Field Topography, 37th Joint Propulsion Conference and Exhibit, American Institute of Aeronautics and Astronautics. https://doi.org/10.2514/6.2001-3890
30. Frieman J, Brown N, Liu C, Liu T, Walker M, Khayms V, King D (2018) Electrical facility effects on Faraday probe measurements. J Propul Power 34(1):267–269. https://doi.org/10.2514/1.B36467
31. Brown DL, Gallimore AD (2011) Evaluation of facility effects on ion migration in a hall thruster plume. https://doi.org/10.2514/1.54143
32. Xu KG (2012) Ion Collimation and In-Channel Potential Shaping Using in-Channel Electrodes for Hall Effect Thrusters, Retrieved 31 March 2024. http://hdl.handle.net/1853/44830
33. Manzella D, Sankovic J Hall (1995) Thruster Ion Beam Characterization, 31st Joint Propulsion Conference and Exhibit, American Institute of Aeronautics and Astronautics. https://doi.org/10.2514/6.1995-2927
34. Kim V (1998) Main physical features and processes determining the performance of stationary plasma thrusters. J Propul Power 14(5):736–743. https://doi.org/10.2514/2.5335
35. Chhavi., Investigation of the Impact of Azimuthal Magnetic Field Gradient on Performance Characteristics and Stability of Hall Effect Thrusters, Dissertation PD (2024) Georgia Institute of Technology
36. Hofer RR, Haas JM, Gallimore AD (2003 Dec) Ion voltage diagnostics in the far-field plume of a high-specific impulse hall thruster NASA/CR–2003-212895

Publisher's note